BOLLETTINO DI GEOFISICA TEORICA ED APPLICATA VOL. 45, N. 3, PP. 187-204; SEPTEMBER 2004

Zoning versus faulting models in PSHA for moderate seismicity regions: preliminary results for the Tricastin nuclear site, France

C. CLÉMENT[1], O. SCOTTI[2], L.F. BONILLA[2], S. BAIZE[2] and C. BEAUVAL[2]

[1] *Ajilon Engineering, Vélizy, France*
[2] *IRSN/DEI/SARG/BERSSIN, Fontenay-aux-Roses, France*

(Received June 6, 2003; accepted January 7, 2004)

Abstract - We are developing a site-specific logic tree approach for a probabilistic seismic hazard assessment at Tricastin, a nuclear site located in the south-east of France, where potentially active faults have been identified. The aim of the logic tree developed in this paper is to compare hazard levels computed according to three main hypotheses (branches) that consider alternative source models (zoning/faulting) as well as alternative seismicity models for the faults (Gutenberg-Richter/characteristic earthquakes). A preliminary exploration of a reduced number of uncertainties, clearly shows that diffuse source zone models lead to hazard results for this site that are higher when compared to fault source models. This holds for short and long return periods and for all spectral values of the ground motion. We attribute this mainly to the source-to-site distance of the fault sources. Indeed, with the exception of a hypothetical blind "fault" modeled near the site, fault sources are all located more than 25 km from the site. Disaggregation results for the Tricastin site of a source zone scenario at 10^{-4} annual probability show that intermediate range magnitudes located at close distances to the site are indeed the controlling events at PGA but at higher spectral periods (0.5 s) greater magnitudes located at larger distances do contribute. Uniform hazard spectra of fault sources show also a significant pseudo spectral acceleration level at central spectral periods for return periods comparable to those of maximum magnitudes. Thus future work requires a more thorough investigation of fault source models.

Corresponding author: O. Scotti, IRSN/DEI/SARG/BERSSIN, B.P. 17, 92262 Fontenay-aux-Roses Cedex, France. Phone: +331 58358647; fax: +331 58358130; e-mail: oona.scotti@irsn.fr

© *2004 OGS*

1. Introduction

The French regulatory commission recommends a deterministic approach to hazard assessments for nuclear power plants (RFS2001-01, 2001; Berge-Thierry et al., 2003a). However, in order to include seismic hazard in a probabilistic safety assessment exercise, we are developing a site-specific probabilistic seismic hazard assessment (PSHA) for the nuclear site of Tricastin (Drôme), located in the south-east of France. France is a country of moderate seismicity where large and destructive earthquakes are rare. For example, the most recent destructive event is the Lambesc 1909 earthquake, with an estimated moment magnitude of *Mw* 6.0 (Baroux et al., 2003). The greatest destructive event in the French catalogue is the 1356 Bâle earthquake near the Swiss-French border with a calculated equivalent local magnitude of 6.2 (Levret et al., 1994). With few major earthquakes and a very diffuse distribution of events recorded in the catalogues, the identification of seismogenic structures and the estimation of their seismic potential remains a challenge. The selection of the Tricastin site for a site-specific PSHA study in France was guided by its location in a region of France where numerous potentially active structures are identified (Baize et al., 2002).

Over the past fifteen years, PSHA studies have undergone a transformation from an approach based mainly on seismological input to an integration of geophysical, geological, and seismological information (e.g. Field et al., 2000). In addition, an important development concerns the quantification of hazard uncertainty through logic tree and Monte Carlo explorations (e.g. Cramer et al., 1996; Wahlström and Grünthal, 2001). According to the most recent developments in this field, we have built a logic tree structure to account for both epistemic and aleatory uncertainties.

Before engaging in an extensive exploration of the uncertainties, we test in this paper a first set of hypotheses in order to identify the ones that will have the greatest impact on the final results. In particular, we compare hazard levels computed by three main branches that consider alternative source and seismicity models. After a brief presentation of the planned full logic tree, we specify, for each level of uncertainty, the options selected for the purpose of the present study. A Monte Carlo exploration of this partial logic tree is then performed, simulating 5,000 seismic hazard scenarios. In the light of the resulting hazard levels that each of these branches produces at the Tricastin site, we then discuss the relative importance of each hypothesis and the future orientations concerning the PSHA study specific to this site.

2. The full logic tree

For the site-specific PSHA study at Tricastin, France, we are developing a logic tree structure that will take into account a full range of uncertainties liable to have an impact on the seismic hazard evaluation at this site: (i) uncertainty due to the methodology used [Cornell (1968), Frankel (1995) and Woo (1996) approaches]; (ii) uncertainty due to the zoning schemes used for the definition of diffuse zones (Autran et al., 1998; GEOTER, 2002 and simplified IRSN's, present study); (iii) uncertainty due to a variety of potential fault sources

scenarios; (iv) uncertainty on magnitude determination of historical and instrumental seismicity; (v) uncertainty due to the use of different magnitude-intensity relationships; (vi) uncertainty due to seismicity models: Gutenberg-Richter (GR), characteristic earthquake (Youngs and Coppersmith, 1985; Wesnousky, 1986); (vii) uncertainty due to the use of different ranges of magnitudes for the calibration of the seismicity models; (viii) uncertainties in source zone parameters such as maximum magnitude, depth and fault source slip rates; (ix) uncertainty due to the choice of attenuation relationships and levels of truncations of their standard deviations; and finally (x) uncertainties due to the choice of the minimum magnitude thresholds considered in PSHA calculations. Given the numerous possible combinations (> 10,000), it is primordial to first identify the important branches. Fig. 1 presents the partial logic tree structure explored for this specific study and the associated hypotheses are explained in the following sections.

3. The logic tree of this study

In the present study PSHA results are obtained using the classical Cornell (1968) method and considering only two seismotectonic models: one describing zones of diffuse seismicity and a second one along specified faults for which two independent seismicity models are proposed. For the purpose of this study the reference EPAS source zoning model (Autran et al., 1998), developed for probabilistic analysis, was re-interpreted (referred to as the simplified IRSN source zone model in Fig. 1). Zones are thus merged to form 10 large seismo-tectonically homogeneous areas of diffuse seismicity (Fig. 2). For the Tricastin zone, the original EPAS

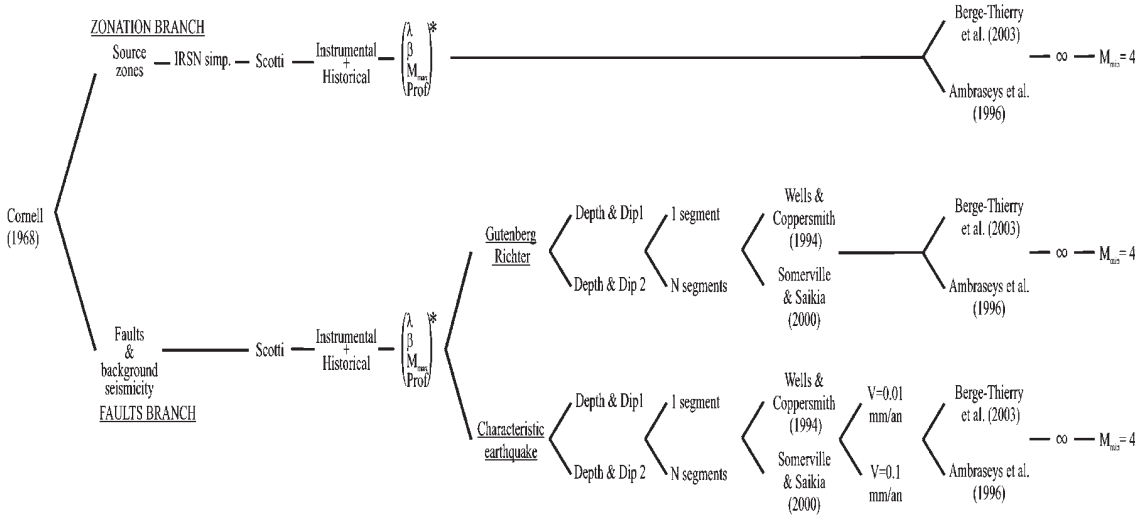

* Seismic parameter uncertainties are explored for λ, β, M_{max} by perturbing the original catalog with a bootstrap method and for depth by random sampling over a uniform distribution

Fig. 1 - Preliminary logic tree constructed for a Monte Carlo exploration of a reasonable number of hypotheses that apply to a PSHA for the site of Tricastin, south-eastern France.

boundaries were modified in order to gather all the main structural features that are characteristic of the French South-East Basin and the associated seismicity in a single zone. In particular, the boundaries are shifted to include the Cévennes fault to the west and to exclude the deformation front related to the Alpine domain.

As can be seen in Fig. 3, fault structures are organized into two families. A family of E-W reverse faults, Lubéron (FL), Ventoux-Lure (FVL), and Trévaresse (CHT) and a family of predominantly NE-SW strike-slip faults, Cévennes (FC), Nîmes (FN), and Durance (FMD). Although there is no evidence of the existence of active faults in the site vicinity, a blind fault, Tricastin (FT), is introduced in this study in order to simulate the existence of repeated moderate earthquakes that occur regularly 7 km north of the Tricastin site (see Fig. 2). The recent activity of the NE-SW and E-W structures is also very poorly documented. Nevertheless, it is possible to propose a history of movement averaged over different geological time windows. Table 1 summarizes the evidence found in the published literature concerning the activity of each of these faults. Slip rates are estimated along most of the structures by averaging the values

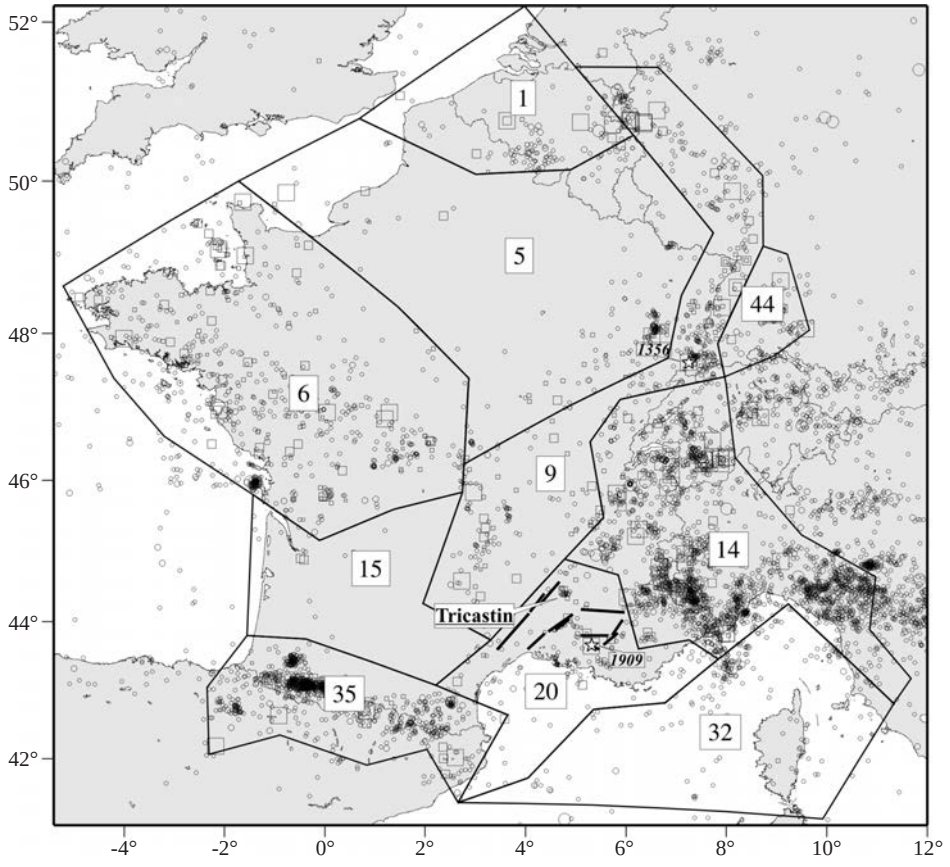

Fig. 2 - The seismogenic source model developed by IRSN for this study. Main active faults, modelled for this PSHA study, are identified within the same zone 20 where the Tricastin site is located. The seismicity catalogue used includes historical seismicity (squares) and the 1962–1999 instrumental seismicity from LDG (circles). The location of the 1909 *Mw* 6.0 Lambesc and the 1356 M_L 6.2 Bâle earthquakes are also shown.

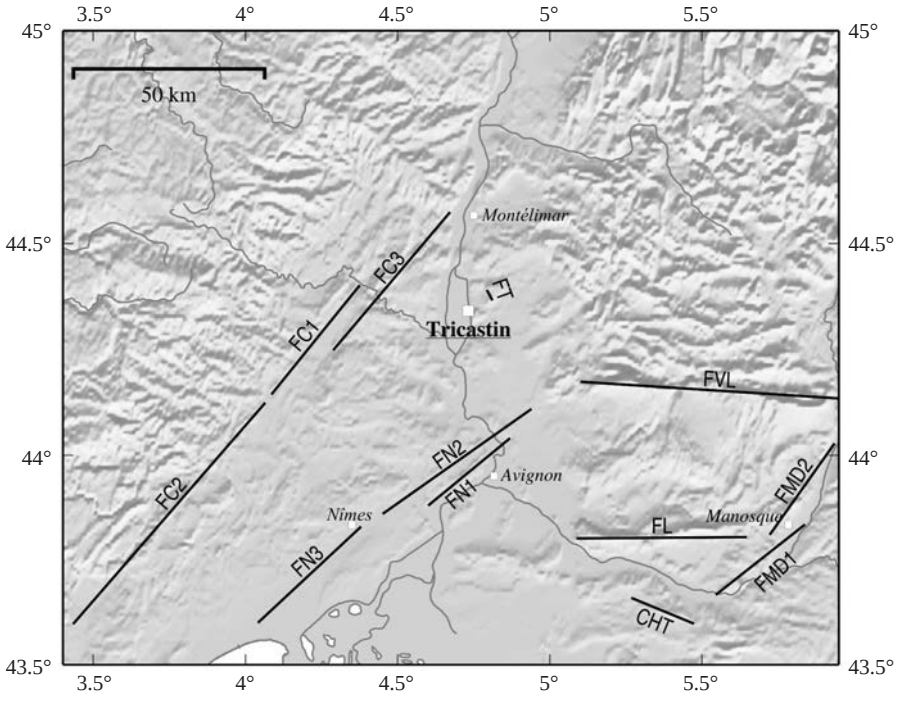

Fig. 3 - Trace of faults modelled in this study: Moyenne Durance (FMD), Nîmes (FN), Cévennes (FC), Ventoux-Lure (FVL), Lubéron (FL), Trévaresse (CHT), Tricastin (FT).

deduced from: (i) Miocene displacements, measuring the long-term deformation rates over 8 million years, (ii) Holocene displacements measured in trenches representative of the last 10,000 years of tectonic activity, and (iii) geodetic rates that are based on the last 4 years of GPS measurements. In this study, the focus is on a direct comparison of seismic hazard levels at the

Table 1 - Bibliographic references used to characterize fault activity (see Fig. 3 for a map location of the faults). The slip rate of FMD fault from GPS data (Calais et al., 2000) is only indicative (recent but unpublished values indicate 0.2 mm/year at most). Present study hypothesis: the slip rate of EW thrust faults (FL, CHT, FVL) was estimated from geological maps on the basis of the vertical displacements of Late Miocene deposits.

Fault	mm/yr	Reference	Type of marker
FMD	0.11	Benedicto (1996)	Miocene vertical displacement
	0.1	Baroux (2000)	Miocene vertical displacement
	0.1	Ghafiri (1995)	Paleoseismic study
	1.3	Calais et al. (2000)	Permanent GPS over 4 years
FN	0.01	Ghafiri (1995)	Paleoseismic study
	0.09	Schlupp et al. (2001)	Miocene horizontal displacement
CHT	0.02	Present study	Miocene vertical displacement
	0.07	Champion (1999)	Balanced cross-section over 10 Myr
FVL	0.1	Present study	Miocene vertical displacement
	0.07	Champion (1999)	Balanced cross-section over 10 Myr
FL	0.1	Present study	Miocene vertical displacement
	0.07	Champion (1999)	Balanced cross-section over 10 Myr
FC	0.1	Lacassin et al. (1998)	Horizontal displacement of terraces
FT	x	x	x

Tricastin site between a diffuse source zone scheme and a fault source approach. In the full logic tree, some background activity rate will also be considered for the fault source branches in order to account for the existence of other potentially active blind faults.

4. Seismicity catalogues

As mentioned previously, numerous magnitude-intensity relationships exist and numerous catalogues can be constructed depending on the method used. Beauval (2003) proposes two historical catalogues deduced on the basis of two magnitude-intensity relationships. The historical magnitudes deduced for the so-called Scotti catalogue are on average 0.4 units higher than those of the so-called Levret catalogue. The choice of the Levret or Scotti catalogue leads to important differences in the resulting hazard (Beauval, 2003) which will be accounted for in the future logic tree. The historical catalogue used in this study is the so-called Scotti catalogue. The combined historical (SISFRANCE, 2001) and instrumental catalogue (provided by the Laboratoire de Détection Géophysique (LDG), CEA, France), not declustered due to the scarcity of identifiable clusters, contains 6460 events with $M_{LDG} \geq 3.0$, 5890 coming from the instrumental period (1962-1999).

In this study, no magnitude conversion is applied, and the magnitudes of the catalogues are assumed to be equal to the M_S magnitude of attenuation relationships. In the future different homogenization schemes will be considered.

An additional level of uncertainty concerns the range of magnitudes that should be used to compute seismicity models. Indeed, Beauval and Scotti (2003a) have shown that the slope of the GR model over the French metropolitan territory is not always independent of the magnitude range used. In other words, the use of instrumental seismicity only, or both instrumental and historical seismicity could lead to different estimates of the GR slope. In this study, the conservative option was chosen where GR seismicity models are computed using both historical and instrumental catalogues, and considering only $M \geq 3.5$. Notice that this threshold corresponds to the minimum magnitude of the catalogue completeness which is not to be confused with the minimum magnitude (damage threshold) of hazard calculations.

5. Variability on the geometry and on the maximum magnitude of fault models

The logic tree (Fig. 1) accounts for two major uncertainties concerning the definition of the fault geometries: their extension at depth and their segmentation at the surface. Guided by alternative interpretations of geological/geophysical cross-sections, an additional uncertainty is provided for some faults (FN, CHT, FMD) by the dip of the structure set as a discrete choice of values. Only the most studied faults profit from a precise mapping of their segmentation at the surface (the FC, the FN, and the FMD faults). For these faults we consider that each segment can rupture individually or together in a cascade type model, leading to multiple scenarios set also as possible discrete choices. For the remaining faults, on the other hand, we have only

considered rupture along a single segment (FVL, FL, CHT). The length of the faults thus depends only on the sampling of the assumed segmentation. The fault width is computed from the assumed dip, chosen among a discrete number of values, and the assumed depth is chosen following a uniform distribution between 5 and 10 km. The total rupture area is then used to determine the maximum magnitude that each fault can support.

The maximum magnitude is calculated using the scaling relationships proposed by Wells and Coppersmith (1994) and Somerville and Saikia (2000), respectively:

$$M = 4.07 + 0.98\ log_{10}(A)$$
$$M = 4.35 + log_{10}(A)$$

where M is the moment magnitude of the maximum characteristic earthquake, and A is the surface of the fault plane. Somerville and Saïka (2000) relationship gives higher estimates of magnitude. The variability (standard deviations) associated to these empirical relations are not integrated for this study; maximum magnitudes vary only with the assumed geometry of the fault. In the future, we might also consider another relationship such as the one recently proposed by Hanks and Bakun (2002) who separate a different tendency for larger magnitudes.

6. Seismicity model

Two different seimicity models are considered, depending on the source type. The doubly-truncated GR seismicity model is considered for the first two branches: diffuse source zones and faults. The third branch considers the characteristic earthquake model, as an alternative seismicity model for faults. Following a Poissonian assumption, the seismicity rates are supposed to be stationary in this study.

7. Diffuse zones and the GR model

The seismicity model attributed to each diffuse source zone is described by a GR relationship doubly truncated between a minimum magnitude threshold (m_0) and a maximum magnitude (m_{max}). We use the following exponential formulation of Cornell and Vanmarcke (1969):

$$\lambda(m) = \lambda_0\ [\exp(-\beta\ (m-m_0)-\exp(-\beta(m_{max}-m_0)]\ /\ [1-\ \exp(-\beta(m_{max}-m_0)] \qquad (1)$$

where λ is the annual activity rate of earthquakes of magnitude m greater than, or equal to, m_0 and lower than m_{max}, λ_0 and β are constants.

Weichert's (1980) method is used, initially to determine the mean λ- and β-values for each zone, and then the associated standard errors. For this study, the completeness periods of

Beauval (2003) are used. Since, in this preliminary study, only source zones with sufficient seismicity are retained, the Aquitaine region (zone 15 in Fig. 2) in the west of France was excluded from the computation.

The seismological parameters (λ_0, β, and maximum magnitude) are varied during the Monte Carlo exploration using a combination of the bootstrap method (Press et al., 1996) and Bayesian technique (Rosenblueth and Ordaz, 1987). We have used a modification of the bootstrap process to take into account the variability on the magnitude estimation. During each iteration, a synthetic catalogue is produced by perturbing 20% of the magnitude data observed in the catalogue. The observed magnitudes in the catalogue were re-sampled using a triangular distribution having a width of 0.25 units. This value was chosen as a lower bound for the magnitude dispersion in both historical and instrumental seismicity data (Beauval and Scotti, 2003a). The a-priori seismological parameters are the ones obtained using Weichert's (1980) method with the corresponding uncertainty on β and λ. The a-priori maximum magnitude is assumed to be 7.0 with a standard deviation of 0.25 for all zones. The Bayesian technique proposed by Rosenblueth and Ordaz (1987) is then used to compute the a-posteriori values for the seismological parameters using the synthetic catalogues. Table 2 shows the maximum and minimum values obtained for each zone. Note that the variability is not very large, which may be due to the small a-priori uncertainties.

The depth of the seismic zones that really affect ground motion estimates only at short distances, is varied within each source zone using the same uniform distribution between 5 and 10 km depth.

8. Fault sources and the GR model

Given the diffuse nature of the seismicity, the number of earthquakes available to compute seismicity models for each of these faults is insufficient. We thus propose to estimate the GR models for each of the faults by distributing the seismic activity rate of the region (λ) along the faults according to their surface area. The region of influence was chosen to cover a square of 200 x 200 km^2 centered on the Tricastin site and including all the identified faults (corresponding

Table 2 - Range of seismicity parameter values explored by the Monte Carlo method for the source-zone branch of the logic tree. λ: activity rate of $4.0 \leq m \leq m_{max}$; β: slope of the GR distribution; m_{max}: maximum magnitude. Depth varies between 5 and 10 km in each zone.

Zone Id	Name	λ (m ≥ 4.0)	β	m_{max}
Zone 1	Nord	3.5e–01-4.4e–01	1.4-1.6	7.2-7.6
Zone 5	Bassin Parisien	3.8e–01-4.4e–01	1.9-2.0	7.0-7.2
Zone 6	Massif Armoricain	1.8e+00-1.9e+00	1.8-1.8	7.2-7.6
Zone 9	Rift	1.0e+00-1.1e+00	1.6-1.7	7.2-7.6
Zone 14	Alpes	4.8e+00-5.0e+00	1.9-2.0	7.2-7.6
Zone 20	SE tricastin	2.1e–01-2.8e–01	1.5-1.7	7.0-7.0
Zone 32	Ligure	4.0e–01-4.6e–01	2.4-2.6	7.0-7.0
Zone 35	Pyrenees	2.9e+00-3.1e+00	2.0-2.0	7.1-7.4
Zone 44	Forêt Noire	7.2e–01-8.4e–01	1.6-1.7	7.1-7.2

to the area of Fig. 3). Then the regional λ-value is shared among the faults according to their surface area. A regional β-value was applied to the seismicity model of all faults. In such a model all faults have the same activity rate per unit surface and capture the entire seismicity of the assumed region of influence.

9. Fault sources and the characteristic earthquake model

The GR model described in the previous paragraph predicts the occurrence of a broad range of possible magnitudes and is based on the catalogue. To investigate an alternative seismicity model for fault sources, the maximum characteristic earthquake model of Wesnousky (1986) is also explored. In this case, an earthquake of the same magnitude repeats itself with a constant recurrence interval. The return periods are estimated based on the slip-rate hypotheses, which were derived from Table 1. Two slip-rate hypotheses are actually considered as limit cases for this study: 0.1 and 0.01 mm/yr. These values are suggested as the upper and lower limits representative of the variability of slip rates when offsets are measured on geological units of different ages. As a first attempt to understand the uncertainty of the chosen parameters for the logic tree branches, we weigh the two slip rate hypotheses equally to all faults independently of their size. We then use Wells and Coppersmith (1994) relation to estimate displacement as a function of the characteristic magnitude:

$$D = \exp[(-5.46+0.82M) \cdot ln(10)] \quad (2)$$

where D is the displacement in meters, and M is the characteristic earthquake moment magnitude also determined by scaling relationships (see previous section on fault geometry and maximum magnitude). The recurrence time of the characteristic earthquake is then deduced from the ratio of the displacement and the assumed slip-rate values. It should be noticed that at each Monte Carlo iteration the computed slip rate differs from one fault to another. On average, a combination of slow and fast slip rates is thus explored.

10. Minimum magnitude and number of standard deviations to be considered in the attenuation models

Two attenuation relationships are set in the logic tree shown in Fig. 1: Ambraseys et al. (1996) and Berge-Thierry et al. (2003b). These two relationships, defined for surface magnitudes, are used because they were recently obtained from the European strong motion database and are the most up-to-date references applicable to the French metropolitan territory. The results presented in this study are conservative, in the sense that no truncation of the probability density function (PDF) of the residual of the attenuation model is considered, and moreover, the minimum magnitude (damage threshold) that is considered for all hazard calculations is $m_0 = 4.0$. In future explorations, we will add more attenuation relationships,

explore the truncation effect between 1σ and no truncation, and the effect of choosing a minimum magnitude value between 4.0 and 5.0, parameter choices which are known to have major impacts on the final hazard estimates (Beauval, 2003).

11. Monte Carlo exploration of the logic tree and hazard calculation

The code used to carry out the hazard calculations was modified from the code CRISIS2000 written by Mario Ordaz (http://www.ifjf.uib.no/Seismologi/software/seisan/seisan.html). The Monte Carlo exploration of the logic tree was programmed by ourselves in Fortran 90 to take into account the complexity of the modeling. At this preliminary stage, in order to understand and quantify the effect of individual branches, we decided to weigh them equally. In this way we do not introduce any preference for any model. At each node there is either a continuous or discrete PDF. Continuous distributions are used for aleatory variables, such as depth (uniform) and magnitude (triangular) whereas discrete distributions, modelled by a Bernoulli distribution, are used for epistemic choices, such as between source models, segmentation options, slip rate options, or again a choice of attenuation relationships. Thus, the result at each iteration corresponds to a random combination of the logic tree branches. The greater the number of iterations there are, the better the exploration of the values at the tail-ends of the distribution. By looking at the evolution of the coefficient of variation (COV) versus the number of iterations, we observed that after 5,000 explorations the COV remains constant. The results of the 5,000 Monte Carlo explorations are presented and classified in Tables 2 to 4 according to their reference model.

12. Results

At each iteration, hazard curves were calculated for probabilities of exceedence ranging from 10^{-1} to 10^{-7}, for peak ground acceleration (PGA) as well as a specified number of spectral periods. Because of the referencing scheme introduced in the calculations, it is easy to select the results according to the different branches and to present results for each individual source. Fig.

Table 3 - Range of parameter values explored by the Monte Carlo method on the fault-source branch of the logic tree assuming a GR model. *R*: distance to the Tricastin site; *L*: length; δ: dip; *Z*: depth; m_{max}: maximum magnitude; λ: activity rate of $4.0 \le m \le m_{max}$; β: the GR-slope varies for all faults in the interval [1.7-1.8].

Fault	R_{min}-R_{max}	L_{min}-L_{max}	δ°	Z_{min}-Z_{max}	m_{max}	λ_{min}-λ_{max} (m≥4)	λ_{min}-λ_{max} (m_{max})
FT	7	4	90°	5-10	5.2 - 5.9	5.0e-05 - 1.1e-04	3.4e-06-7.9e-06
FC	26 - 128	38-133	70°	5-10	6.3 - 7.5	4.3e-04 - 3.9e-03	4.1e-06-1.5e-05
FN	30 - 99	27- 92	70°/40°	5-10	6.2 - 7.5	3.2e-04 - 7.3e-03	3.7e-06-2.8e-05
FVL	34 - 100	69	45°	5-10	6.7 - 7.3	2.2e-03 - 4.7e-03	9.8e-06-2.6e-05
FL	66 - 88	36	45°	5-10	6.5 - 7.2	1.4e-03 - 3.0e-03	9.0e-06-2.3e-05
CHT	87 - 102	18	45°/70°	5-10	6.0 - 6.8	2.0e-04 - 1.2e-03	3.4e-06-1.8e-05
FMD	99 - 105	30- 50	45°/70°	5-10	6.2 - 7.2	3.4e-04 - 3.4e-03	3.8e-06-2.3e-05

Table 4 - Range of parameter values explored by the Monte Carlo method on the fault-source branch of the logic tree assuming a characteristic earthquake model. *R*: distance to the Tricastin site; *L*: length; δ: dip; *Z*: depth; *M*: characteristic maximum magnitude derived from scaling relationships as a function of the rupture area; *T* and λ: return period and corresponding annual rate of earthquake of *M*.

Fault	R_{min}-R_{max}	L_{min}-L_{max}	δ°	Z_{min}-Z_{max}	M_{min}-M_{max}	T_{min}-T_{max}	λ_{min}-λ_{max}
FT	7	4	90°	5-10	5.2 – 5.9	703 - 21731	4.6e-05 - 1.4e-03
FC	26 - 128	38 -133	70°	5-10	6.3 – 7.5	5372 - 530170	1.9e-06 - 1.9e-04
FN	30 - 99	27 - 92	70°/40°	5-10	6.2 – 7.5	4243 - 491472	2.0e-06 - 2.4e-04
FVL	34 - 100	69	45°	5-10	6.7 – 7.3	11090 - 364790	2.7e-06 - 9.0e-05
FL	66 - 88	36	45°	5-10	6.5 – 7.2	7730 - 253452	3.9e-06 - 1.3e-04
CHT	87 - 102	18	45°/70°	5-10	6.0 – 6.8	2952 - 119408	8.4e-06 - 3.4e-04
FMD	99 - 105	30 - 50	45°/70°	5-10	6.2 – 7.2	4447 - 279939	3.6e-06 - 2.2e-04

4 shows the mean, 16th, 50th and 84th percentiles PGA hazard curves calculated from the distribution of accelerations resulting from each of the three main branches: diffuse zones, faults with GR model, and faults with characteristic model. The diffuse zones source model leads to the highest hazard levels at all return periods. Conversely, the hazard curves of the fault branches are completely dominated by the modelling of the nearby Tricastin fault (compare Figs. 4a and 4b). The area of their 16th to 84th percentiles outlines the variability of each model. Fault models with characteristic earthquakes show a greater dispersion, which is controlled by the details of the fault geometry used to compute the magnitude, and in particular, the wide range of assumed slip rates. GR models, on the other hand, present a much narrower dispersion independently of fault or diffuse seismicity zone hypotheses. For the GR model, the observed

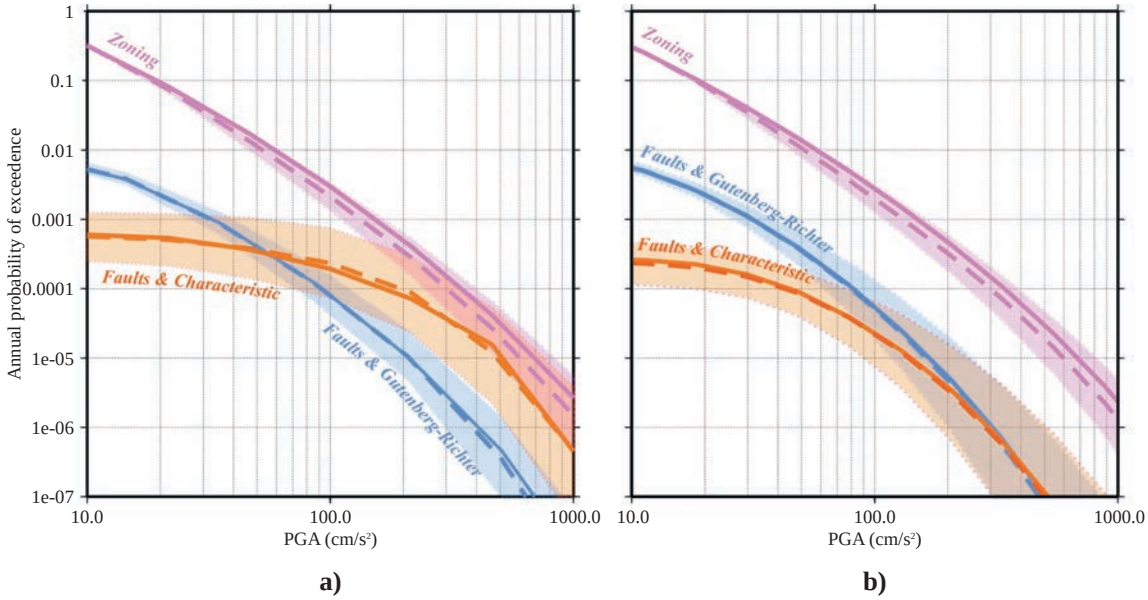

Fig. 4 - Median (plain) and mean (dashed) hazard curves with their associated variability, 16th and 84th percentile (shadow) resulting from 5,000 Monte Carlo simulations of the logic tree. Curves are shown for individual branches: pink for the zoning branch, blue for the fault branch with GR model and orange for the fault branch with characteristic earthquake model. The influence of the nearby FT for both fault branches is clearly illustrated by their respective hazard curves with (a) and without (b) the contribution of this fault.

variability using this logic tree configuration mainly depends on the explored depth range (Tables 2 and 3). The details of the geometry and of the seismicity model assumed for the nearby FT fault source play a key role in the resulting seismic hazard at Tricastin.

But how does the hazard resulting from the remaining fault sources compare between the two fault branches? Fig. 5 shows a direct comparison between the two fault branches excluding the contribution of the FT source. In addition, the contribution of each individual fault source is extracted. Nearby faults FVL, FC, FN, and FL contribute almost equally to the total hazard level of the GR fault branch represented by the upper red curve and its 68% confidence limits (shaded area). Conversely, far-away faults CHT and FMD contribute the least. Thus, the main parameter controlling the hierarchy of the hazard curves appears to be the fault-to-site distance (Table 3), as already suggested by the FT fault in Fig. 4a.

Fig. 5b, shows the results for the characteristic earthquake model. The total hazard level in this branch is lower than the GR-fault model (Fig. 5a), except for very small annual probabilities of exceedence. Nonetheless, it is observed that the distant CHT fault contributes largely to the total hazard of this branch up to 10^{-5} annual probability of exceedence. At the other end, the nearby FVL fault contributes the least (Table 4). This rather unexpected hierarchy, compared to Fig. 5a, is controlled by the fact that in the proposed characteristic earthquake model, small fault segments such as the CHT, produce small events that dominate the hazard even at such small annual probability levels (remember that no truncation of the attenuation relationship is applied in this study). Future modelling efforts will focus on estimating fault specific slip-rate hypotheses.

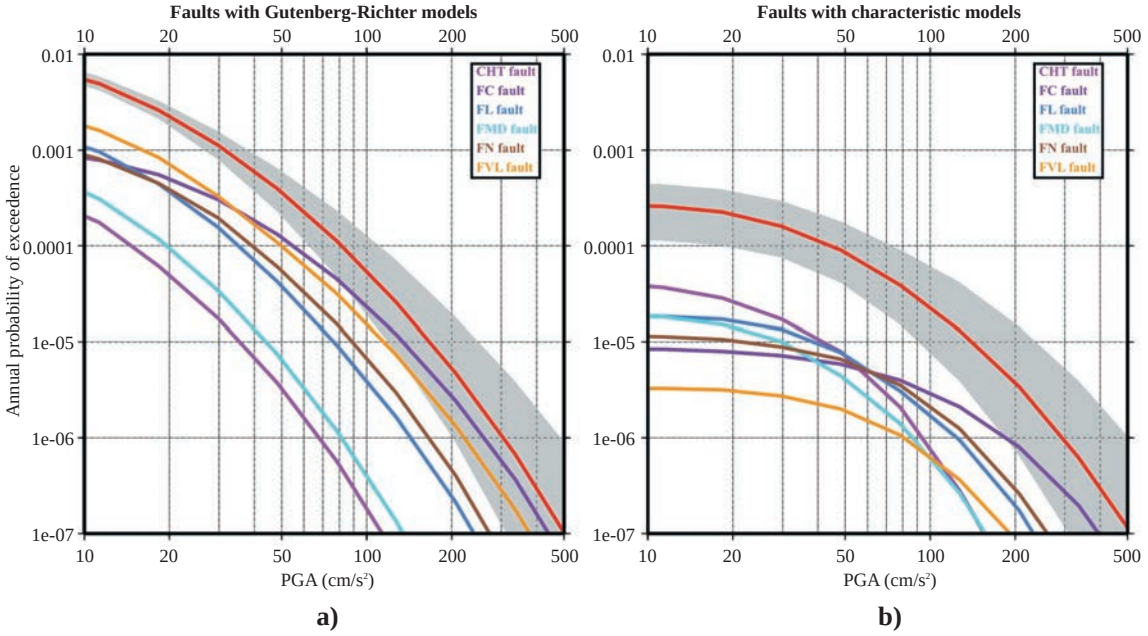

Fig. 5 - Comparison between the GR (a) and characteristic earthquake (b) models for the fault branches. The red curves are the same mean hazard curves reported in Fig. 4b with their corresponding 16th to 84th percentiles hazard levels (shadow). Other colored curves correspond to the mean hazard contribution of individual faults (the FT fault, is not considered here).

13. Discussion

In spite of the simple assumptions considered in the present study, seismic hazard at the Tricastin site clearly appears to be controlled by the diffuse source-zone models rather than the fault-source models. Nevertheless, the existence of a hypothetical blind fault (FT) located at 7 km north of the site, with a seismicity distribution fitting a characteristic model, can lead to comparable hazard levels beginning at a 10^4 - year return period. The contribution coming from the remaining faults, that are all more than 25 km away from the site, may change with a wider exploration of potential scenarios and assumed slip rates that are in better agreement with those described in Table 1.

It is interesting to compare the influence of the two seismicity models on the hazard levels of each individual fault source (Fig. 5). In spite of the very different hypotheses, the constant activity rate/per surface area approach (GR model), and the slip rates approach (characteristic model) lead to very similar hazard levels going towards large return periods. At lower return periods, the GR approach produces higher hazard levels and yet the characteristic model produces, on average, higher rates of maximum magnitudes (compare last column in Table 3 and Table 4). This indicates that intermediate and lower magnitudes provide the greatest amount of hazard in the GR model. This effect is particularly clear for the FVL fault. No segmentation is actually defined for this fault which is thus one of the longest and has a site-to-fault distance of only 30 km. The magnitude explored with the GR model for this fault ranges from 4.0 to 6.7-7.3 whereas the range explored with the characteristic model is 6.7-7.3. Even, if the FVL fault catches a big proportion of the activity rate due to its large area, the annual rate of maximum magnitude stays on average lower with the GR model than with the characteristic earthquake model. Finally, the contribution of this fault is much more important in the GR model because of the more frequent occurrence of lower magnitudes. The opposite behavior is observed for the shortest and farthest CHT fault. Its preponderant role, at probability levels of less than 10^{-5} in the characteristic model, is due to the shorter return period of its maximum magnitude. Finally both cases illustrate the influence of an intermediate magnitude range for the PGA at shorter return periods.

Furthermore, it will be important to consider not only PGA hazard curves but also other spectral periods. Fig. 6 shows the uniform hazard response spectrum (UHS) at a return period of 10^4 years for the three branches, again, ignoring the FT fault source in the fault branches. What we can see is that even for 10^4 years, that can start to be comparable with the return periods of characteristic earthquakes, the hierarchy between models is the same as for the PGA levels. The diffuse zone model remains the greatest contributor for all frequencies and all return periods. The UHS levels of the characteristic fault model become comparable or even higher than those due to the GR-fault model only for return periods beyond 10^5 years (not shown here). However, pseudo-acceleration of fault models can reach significant levels (> 0.1g) for lower spectral periods. Thus, the modelling of active faults may be important for return periods of 10^4 years and beyond, since their contribution may affect the shape of the low-frequency uniform hazard spectrum.

In Fig. 7a, the (M,d,ε) disaggregation of a mean hazard PGA scenario of 0.33 g in the source-zone model branch, corresponding to probabilities of exceedence of 10^{-4} (Fig. 4), clearly

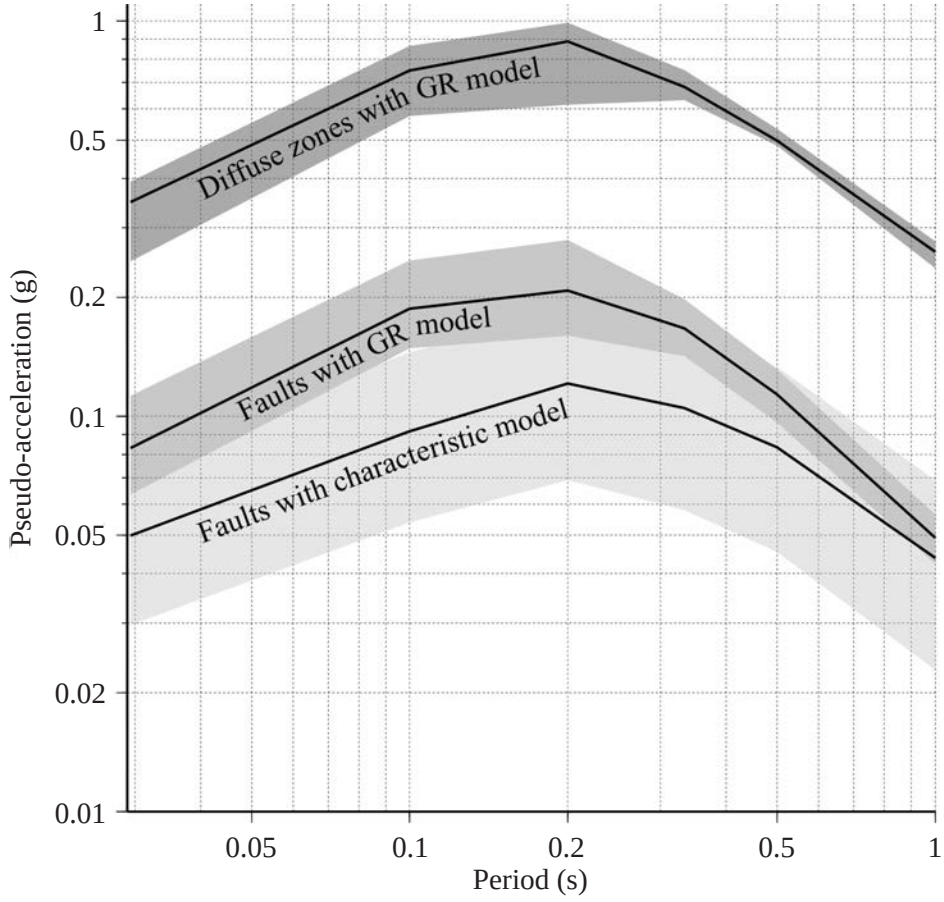

Fig. 6 - UHS calculated at the Tricastin site for a return period of 10^4 years. The curves with their grey area show the calculated mean spectral accelerations and their associated variability (16^{th} to 84^{th} percentiles) expected to be exceeded with a 10^{-4} annual probability. Each curve results from the exploration of one of the three main branches presented in Fig. 1. For all spectral periods the diffuse source zone model produces higher levels of hazard compared to both fault models (FT is ignored).

shows that most of the hazard contribution for the site of Tricastin comes from distances of less than 30 km. This scenario also illustrates that intermediate magnitudes indeed play an important role and that the maximum magnitude bin [7.0 – 7.5] contributes the least to the hazard level. The same mean scenario produces spectral acceleration of PSA = 0.46 g for 0.5 s spectral period at probabilities of exceedence of 10^{-4}. A disaggregation for this spectral period (Fig. 7b) shows that sources located at distances beyond 30 km contribute to the hazard and that the maximum magnitude plays an important role at these frequencies. This result again indicates that sources at larger distances than the local scale around the site could influence the hazard level at higher spectral periods (Beauval and Scotti, 2003b).

Notice also that the contribution to the resulting hazard level comes from probabilities beyond one standard deviation from the median value of the attenuation model. The absence of truncation in the PDF attenuation model residual implies that low probability movements ($\varepsilon > 1\sigma$) can contribute or may even dominate the hazard levels, giving unrealistic values for

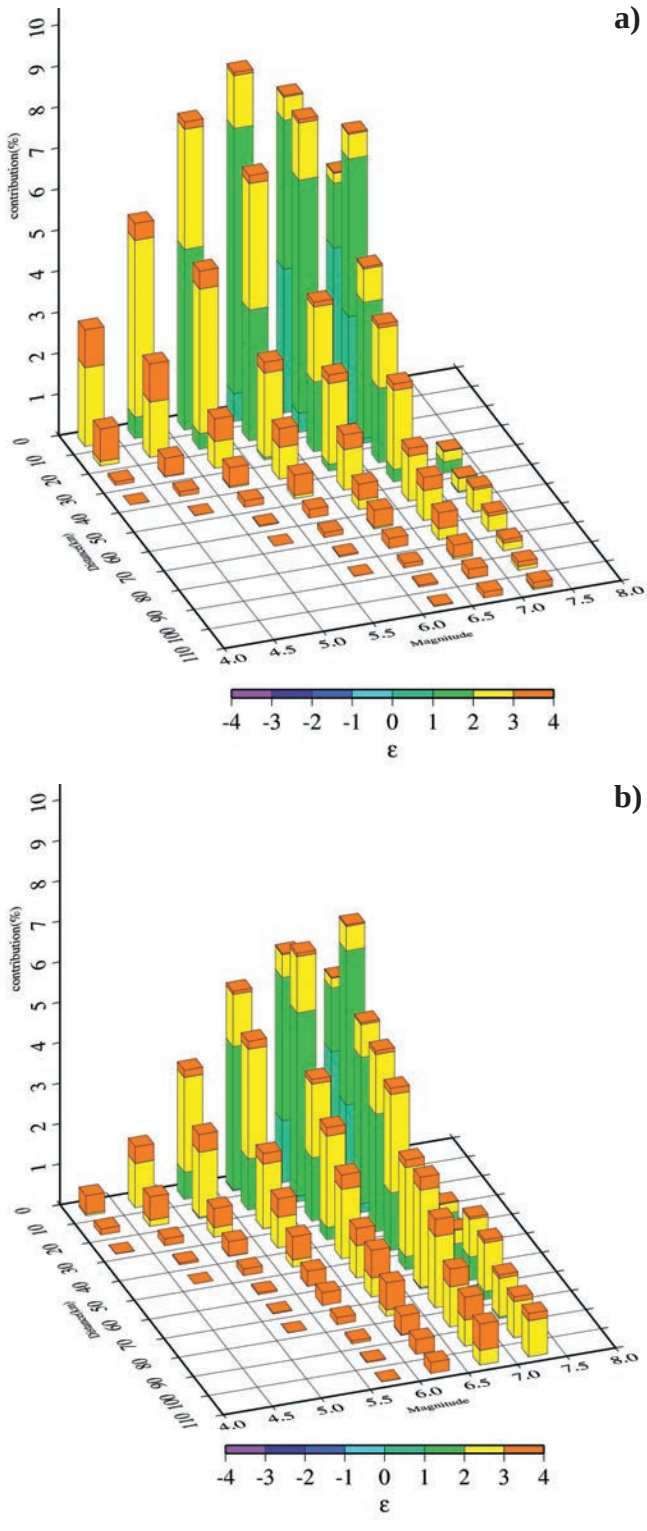

Fig. 7 - Disaggregation of a source zone scenario at the Tricastin site: a) PGA (34 Hz, 5%) = 0.33 g; and b) PSA (2 Hz, 5%) = 0.46 g, equivalent to the mean hazard levels given by the zoning branch at 10^{-4} annual probability. Note that for a lower spectral period (b) the contribution of larger distances and of greater magnitudes increases.

design ground motion. Future work will have to consider the truncation of the PDF attenuation relationship residual, depending on the specific objective of the PSHA study.

14. Conclusions

We have developed a site-specific probabilistic seismic hazard methodology for the nuclear power plant of Tricastin, located in the south-east of France. The methodology involves the definition of a logic tree, taking into account a full range of uncertainties. In this preliminary study, we have selected a subset of hypotheses to compare the impact of three main seismotectonic models. One branch of the partial logic tree tests the occurence of diffuse seimicity distributed in source zones. Assuming either a GR or a characteristic earthquake distribution of magnitudes, two other branches consider the seismicity localized on specified faults. A Monte Carlo approach is used to simulate 5,000 seismic scenarios combining the different uncertainties set in our logic tree. In the three branches, we explore, in particular, the variability of the activity parameters, different geometries and slip rates for the fault models, the depth of the sources and two attenuation relationships.

Given the configuration of the faults, all located beyond 25 km from the Tricastin site, we show that for all return periods and for all spectral periods the mean hazard curve computed on scenarios of diffuse seismicity always reaches hazard levels higher than any fault model. Only a hypothetical blind fault (FT fault), tested to model the so-called Tricastin swarm located at 7 km north of the site, could produce a nearly comparable hazard at large return periods. However, we considered for this fault a fairly unrealistic model for the characteristic earthquakes with a maximum slip rate of 0.1 mm/yr, which is more appropriate for the main structures in the region. For the future PSHA study, we may wonder, if fault models for the Tricastin site need to be considered at all. However, the UHS at return periods larger than 10^4 years indicates that even if the hazard level is always lower compared to diffuse source zones, faults are bringing significant hazard level greater than 0.1g for central spectral periods. Since we are concerned with annual probability levels as small as 10^{-5}, of the order of the periodicity of characteristic earthquakes on the faults, their increasing contribution cannot be ignored, as they can influence the shape of the uniform hazard spectrum for central spectral periods.

Acknowledgments. The present study was carried out in the framework of the Institut de Radioprotection et de Sûreté Nucléaire (IRSN) project “Probabilistic Safety Assessment of nuclear power plants in France” under contract IRSN/ 21000690. We thank reviewers and editors for constructive comments. Special thanks go to M. Ordaz (UNAM, University of Mexico) for providing us with the source code Crisis2000.

References

Autran A., Blès J.L., Combes Ph., Cushing M., Dominique P., Durouchoux Ch., Gariel J.C., Goula X., Mohammadioun B. and Terrier M.; 1998: *Probabilistic seismic hazard assessment in France: part one: seismotectonic zonation.* In: Proc. 11th Europ. Conf. on Earth. Eng., CD-ROM, Paris, Sept. 1998.

Ambraseys N.N., Simpson K.A. and Bommer J.J.; 1996: *Prediction of horizontal response spectra in Europe.* Earth. Eng. and Struct. Dyn., **25**, 371-400.

Baize S., Cushing E.M., Lemeille F., Granier T., Grellet B., Carbon D., Combes P. and Hibsch C.; 2002: *Inventaire des indices de rupture affectant le Quaternaire en relation avec les grandes structures connues, en France métropolitaine et dans les régions limitrophes.* Mém. Soc. Géol. Fr., H.S., **175**, 142 pp.

Baroux E.; 2000: *Tectonique active en région à sismicité modérée : le cas de la Provence (France). Apport d'une approche pluridisciplinaire.* PhD thesis, Univ. Orsay, 327 pp.

Baroux E., Pino N.A., Gianluca V., Scotti O. and Cushing M.E.; 2003: *Source parameters of the 11 June 1909, Lambesc (Provence, southeastern France) earthquake: a reappraisal based on macroseismic, seismological, and geodetic observations.* J. Geophys. Res., **108**, B9, 2454, doi: 10.1029/2002JB002348.

Beauval C.; 2003: *Analyse des incertitudes dans une estimation probabiliste de l'aléa sismique, exemple de la France.* PhD thesis, Univ. J. Fourier, Grenoble, 168 pp.

Beauval C. and Scotti O.; 2003a: *Mapping b-value in France using two different magnitude ranges: possible non power-law behavior.* Geophys. Res. Lett., **30**, 17, 1892, doi: 10.1029/2003GL017576.

Beauval C. and Scotti O.; 2003b: *Quantifying uncertainties in French PSHA due to catalogue uncertainties, ground motion dispersion and choice of magnitude range.* Bull. Seism. Soc. Am., submitted.

Benedicto A.; 1996: *Modèles tectono-sédimentaires de bassins en extension et style structural de la marge passive du Golfe du Lion (partie nord), sud-est de la France.* PhD thesis, Univ. Montpellier, 235 pp.

Berge-Thierry C., Scotti O. and Bonilla F.; 2003a: *Seismic hazard assessment in France and associated uncertainties.* In: Proceedings of the International Symposium on seismic evaluation of existing nuclear facilities, Vienna, pp 38-42.

Berge-Thierry C., Cotton F., Scotti O., Griot-Pommera D.A. and Fukushima Y.; 2003b: *New empirical response spectral attenuation laws for moderate European earthquakes.* J. Earth. Eng., **7**, 193-222.

Calais E., Galisson L., Stéphan J.-F., Delteil J., Deverchère J., Larroque C., Mercier de Lépinay B., Popoff M. and Sosson M.; 2000: *Crustal strain in the Southern Alps, France, 1948-1998.* Tectonoph., **319**, 1-17.

Champion C.; 1999: *Déformation de la Provence occidentale depuis le Miocène. Étude structurale, utilisation des surfaces géomorphologiques marqueurs et analyse quantitative du relief.* PhD thesis, Univ. Aix-Marseille III, 213 pp.

Cramer C.H., Petersen M.D. and Reichle M.S.; 1996: *A Monte Carlo approach in estimating uncertainty for a seismic hazard assesment of Los Angeles, Ventura, and Orange Counties, California.* Bull. Seism. Soc. Am., **86**, 1681-1691.

Cornell C.A.; 1968: *Engineering seismic risk analysis.* Bull. Seism. Soc. Am., **58**, 1583-1606.

Cornell C.A. and Vanmarcke E.H.; 1969: *The major influences on seismic risk.* In: Proc. Fourth World Conf. on Eq. Eng., Santiago, **A-1**, pp. 69-93.

Field E.H. and SCEC Phase III Working Group; 2000: *Accounting for site effects in probabilistic seismic hazard analyses of Southern California: Overview of the SCEC Phase III Report.* Bull. Seism. Soc. Am., **90**, 1-31.

Frankel A.; 1995: *Mapping seismic hazard in the Central and Eastern United States.* Seism.Res. Lett., **66**, 8-21.

Ghafiri A.; 1995: *Paléosismicité de failles actives en contexte de sismicité modérée: application à l'évaluation de l'aléa sismique dans le Sud-Est de la France.* PhD thesis, Univ. Paris XI, 337 pp.

GEOTER; 2002: *Révision du zonage sismique de la France - Etude probabiliste.* Rapport GTR/MATE/701-150, 18 août.

Hanks T.J. and Bakun W.H.; 2002: *A bilinear source-scaling model for M–logA observations of continental earthquakes.* Bull. Seism. Soc. Am., **92**, 1841-1846.

Lacassin R., Meyer B., Benedetti L., Armijo R. and Tapponnier P.; 1998: *Signature morphologique de l'activité de la faille des Cévennes (Languedoc, France).* C. R. Acad. Sci., **326**, 807-815.

Levret A., Backe J. and Cushing M.; 1994: *Atlas of macroseismic maps for French earthquakes with their principal characteristics.* Natural Hazards, **10**, 19-46.

Press W.H., Teukolsky S.A., Vetterling W.T. and Flannery B.P.; 1996: *Numerical recipies in FORTRAN 77: the art of scientific computing.* Cambridge University press, Second Edition, 963 pp.

Rosenblueth E. and Ordaz M.; 1987: *Use of seismic data for similar regions.* Earth. Eng. and struc. dyn., **15**, 619-634.

RF 2001-01; 2001: *La règle fondamentale de sûreté (RFS) n°2001-01 relative à la détermination du risque sismique pour les installations nucléaires de base à l'exception des stockages à long terme de déchets radioactifs.* http://www.asn.gouv.fr/data/information/decision12a.asp, DSIN-GRE/SD2/ n°79/2001.

SISFRANCE; 2001: *http://www.sisfrance.net*.

Somerville P. and Saikia C.; 2000: *Ground motion attenuation relations for the Central and Eastern United States.* Progress Report to the USGS, January 28, 2000, URS Greiner Woodward Clyde, Pasadena; 10 pp.

Schlupp A., Clauzon G. and Avouac J.-P.; 2001: *Mouvement post-messinien sur la faille de Nîmes: implications pour la sismotectonique de la Provence.* Bull. Soc. Géol. Fr., **172**, 697-712.

Walhström R. and Grünthal G.; 2001: *Probabilistic seismic hazard assessment (horizontal PGA) for Fennoscandia using the logic tree approach for regionalization and nonregionalization models.* Seism. Res. Let., **72**, 33-45.

Weichert D.H.; 1980: *Estimation of the earthquake recurrence parameters for unequal observation periods for different magnitudes.* Bull. Seism. Soc. Am., **70**, 1337-1346.

Wells D.L. and Coppersmith K.J.; 1994: *New empirical relationships among magnitude, rupture length, rupture width, rupture area, and surface displacement.* Bull. Seism. Soc. Am., **84**, 974-1002.

Wesnousky S.G.; 1986: *Earthquakes, Quaternary faults, and seismic hazard in California.* J. Geophys. Res., **91**, 12,587-12,631.

Woo G.; 1996: *Kernel estimation methods for seismic hazard area source modeling.* Bull. Seism. Soc. Am., **86**, 353-362.

Youngs R.R. and Coppersmith K.J.; 1985: *Implications of fault slip rates and earthquake recurrence models to probabilistic seismic hazard estimates.* Bull. Seism.Soc. Am., **75**, 939-964.